

**Non-Markovian enhancement of nonequilibrium quantum thermometry**Y. Aiache <sup>1,\*</sup> C. Seida <sup>1,2</sup> K. El Anouz <sup>1</sup> and A. El Allati <sup>1,3</sup><sup>1</sup>Laboratory of R&D in Engineering Sciences, Faculty of Sciences and Techniques Al-Hoceima, *Abdelmalek Essaadi University*, BP 34, Ajdir 32003, Tetouan, Morocco<sup>2</sup>ESMaR, Faculty of Sciences, *Mohammed V University* in Rabat, B.P. 1014 Rabat, Morocco<sup>3</sup>Max Planck Institute for the Physics of Complex Systems, Nöthnitzer Strasse 38, D-01187 Dresden, Germany

(Received 17 March 2024; accepted 30 July 2024; published 23 August 2024)

Accurate measurement at low temperatures is essential for both gaining a fundamental understanding of physical processes and developing technological applications. In this paper, we propose a theoretical framework for quantum temperature sensing in a composite environment with non-Markovian dynamics. Our suggested system uses a single qubit as a temperature sensor to test its sensitivity in calculating the temperature of a composite environment. We show that the temperature sensor's sensitivity can saturate the quantum Cramér-Rao bound by measuring the  $\hat{\sigma}_z$  observable of the probe qubit. Temperature sensing performance is measured using the quantum signal-to-noise ratio. We underline how non-Markovianity can enhance the performance of our thermometers. Furthermore, we emphasize that nonequilibrium conditions do not always result in the best sensitivities in temperature estimation.

DOI: [10.1103/PhysRevE.110.024132](https://doi.org/10.1103/PhysRevE.110.024132)**I. INTRODUCTION**

Directly measuring the properties of quantum mechanical systems is frequently difficult or unfeasible. Moreover, in many circumstances, any attempt at direct disturbance may change the properties of the system, potentially jeopardizing its basic features. To overcome this constraint, there is rising interest in creating efficient strategies for indirect quantum probing [1]. One use is quantum thermometry, which involves estimating a quantum system's operational temperature. This subject offers intriguing opportunities for the design and implementation of indirect probing strategies, notably for the characterization and control of the temperature of micro- and nanodevices [2–6]. Quantum thermometry, as a promising area of quantum metrology, has the potential to address low-temperature measurements through the use of quantum thermometers [7–12]. In this context, an ideal quantum thermometer should be significantly smaller than the sample to be measured. Recently, attention has focused on two-level quantum systems, or qubits, as the smallest and most versatile thermometers [13–17]. This approach has been successfully demonstrated in several settings, including ultracold gases [18].

In addition, quantum parameter estimation theory provides vital instruments for determining the ideal initial preparation state of the probe, i.e., the thermometer. Indeed, it develops

appropriate strategies for performing optimal measurements on the probe's output state in order to achieve the bound of estimation accuracy. It is worth noting that the results of these ideal measurements on the probe's output state are utilized to create an operator or estimator, which provides direct access to parameter information. Quantum Fisher information (QFI) [19–21] is a commonly used tool in quantum parameter estimation theory. The QFI is important in parameter estimation since it is closely related to the ultimate limit on achievable precision when estimating an unknown parameter, as demonstrated by the quantum Cramér-Rao bound [19]. Quantum Fisher Information can be used to detect quantum phase transitions in many-body systems [22,23], quantify the smallest evolution time for a quantum process [24,25], and measure non-Markovian information flow in an open quantum system [26–29].

In this paper, we provide a theoretical model for constructing a thermometer using a single qubit as the sensing probe. The suggested model includes a two-level system (probe qubit) that interacts with a composite environment. The composite environment represents the sample under inquiry and can cause non-Markovianity on the probe qubit. In particular, the composite environment is divided into two parts: an ancilla and a Markovian reservoir. We obtain the combined state of the qubit and ancilla by solving the master equation exactly. In this method, the qubit encodes temperature information from the thermally composite environment into the state of the probe, also known as the thermometer. The performance of temperature sensing is evaluated using the quantum signal-to-noise ratio (QSNR) metric [19]. After allowing the qubit to interact with its environment, we use a measurement of  $\hat{\sigma}_z$  to derive temperature information. Our findings indicate that, in nonequilibrium conditions, increasing non-Markovianity improves QSNR with numerous

\*Contact author: [youssefaiache0@gmail.com](mailto:youssefaiache0@gmail.com)

Published by the American Physical Society under the terms of the [Creative Commons Attribution 4.0 International](https://creativecommons.org/licenses/by/4.0/) license. Further distribution of this work must maintain attribution to the author(s) and the published article's title, journal citation, and DOI.

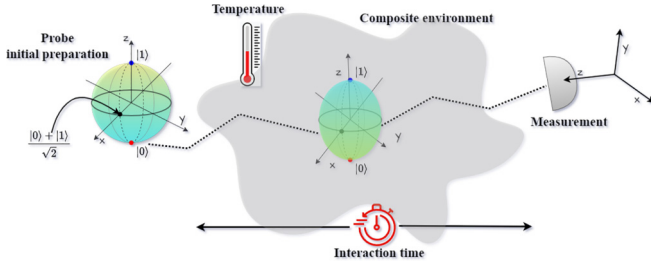


FIG. 1. Illustration of the physical system being studied: A two-level system interacts with a thermally composite environment, which works as a quantum thermometer to determine its temperature. Our probe process goes as follows: First, we set the probe qubit to the optimal state represented by the Bloch sphere. The probe qubit then interacts with the composite environment to encode temperature information. Finally, we perform a measurement of  $\hat{\sigma}_z$ , which is suitable for saturating the quantum Cramér-Rao constraints.

oscillations, whereas in the Markovian regime, QSNR grows slowly. However, equilibrium conditions yield the most accuracy. Overall, our proposed method performs exceptionally well in the low-temperature range. We also investigate the scenario in which the composite environment has varying temperatures. The study focuses on calculating the temperature of the ancilla in the presence of various Markovian reservoir characteristics and memory effects.

This paper is organized as follows: Sec. II provides a brief overview of the approaches from local quantum estimating theory (QET) that will be used throughout this study. Section III describes our physical model and characterizes the probe qubit's non-Markovianity. Sections IV and V discuss the application of QET approaches to our system, giving our findings and illustrating the achievement of optimal estimation using feasible measurements. Finally, Sec. VI concludes the paper with some final statements.

## II. TOOLS FOR QUANTUM PARAMETER ESTIMATION THEORY

Direct access to essential physical quantities is frequently unavailable in various sensing techniques, necessitating indirect measurement estimates. In such instances, the purpose of estimate theory is to precisely infer the value of the desired quantity by studying a set of data obtained from measuring another observable.

We begin by examining the fundamentals of quantum thermometry. We intend to estimate temperature, which is a parameter rather than a quantum observable, using measurements on the probe in our approach (see Fig. 1). QFI is an important part of parameter estimation theory since it offers a measure of the maximum precision that can be achieved in a thermometry scheme. The ultimate precision of an unbiased temperature estimator  $\hat{T}$  follows the quantum Cramér-Rao (QCR) theorem, which asserts that

$$\Delta T \geq \Delta T_{\text{QCR}} \geq 1/\sqrt{\nu \mathcal{H}(T)}, \quad (1)$$

where  $\Delta T$  is the mean square error,  $\nu$  is the number of measurements, and  $\mathcal{H}(T)$  is the quantum Fisher information of the probe state  $\rho^{(P)}$ , which varies with the temperature of the

composite environment. The QFI is defined in the following manner:

$$\mathcal{H}(T) = \text{Tr}\{\rho^{(P)}(T)L^2(T)\}, \quad (2)$$

where  $L^2(T)$  is the symmetric logarithmic derivative operator satisfying the equation

$$2\partial_T \rho^{(P)}(T) = L(T)\rho^{(P)}(T) + \rho^{(P)}(T)L(T), \quad (3)$$

where  $\partial_T$  denotes the temperature-dependent derivative. As seen in Fig. 1, the quantum thermometer is a single qubit probe that interacts with the composite environment. In particular, note that for a two-dimensional quantum probe, any qubit state in the Bloch sphere representation can be expressed as  $\hat{\rho} = \frac{1}{2}(\hat{I} + \mathbf{b} \cdot \hat{\boldsymbol{\sigma}})$ , where  $\hat{I}$  is the  $2 \times 2$  identity matrix,  $\mathbf{b} = (b_x, b_y, b_z)$  is the real Bloch vector, and  $\hat{\boldsymbol{\sigma}} = (\hat{\sigma}_x, \hat{\sigma}_y, \hat{\sigma}_z)$  represents the Pauli matrices. In this situation, the quantum Fisher information can be expressed for any mixed state by

$$\mathcal{H}(T) = |\partial_T \mathbf{b}|^2 + \frac{(\mathbf{b} \cdot \partial_T \mathbf{b})^2}{1 - |\mathbf{b}|^2}. \quad (4)$$

The performance of temperature sensing can be described by the quantum signal-to-noise ratio which will be used throughout this paper, and it defined as

$$\mathcal{R}_T = T^2 \mathcal{H}(T). \quad (5)$$

Using the QCR bound in Eq. (1) and the QSNR in Eq. (5), the optimal relative error and the QSNR show the following relationship:

$$\frac{(\Delta T)_{\min}}{T} = \frac{1}{\sqrt{\nu \mathcal{R}_T}}, \quad (6)$$

which means that the higher QSNR allows more accurate temperature sensing.

In the following section, we will use the framework mentioned above to estimate the temperature  $T$  of the sample with either Markovian or non-Markovian dynamics. The estimation approach includes the interaction of a qubit with the sample, followed by measurements to calculate the temperature. Specifically, we investigate an entirely solvable variant of the master equation in order to build an effective quantum thermometry method.

## III. PROPOSED MODEL AND DYNAMICS

### A. The physical model

All quantum physical systems interact with their surroundings, which distinguishes them as actual physical systems. Their interactions with the surrounding environment frequently result in a loss of coherence and information [30–32]. This phenomenon can be leveraged to transform the quantum system into an effective probe for estimating various environmental factors. Before getting into the technicalities of quantum thermometry, we present a thorough description of the environment, which we regard as a composite environment. This organized reservoir produces non-Markovian dynamics on the probe [33]. It consists of two components: a Markovian thermal reservoir and a two-level system known as an ancilla. Figure 1 shows a schematic diagram of our quantum thermometry probing approach.

The Hamiltonian governing the system of interest is expressed as (we adopt units of  $\hbar = 1 = k_B$  throughout this study)

$$H = \omega^P \sigma_+^P \sigma_-^P + \omega^A \sigma_+^A \sigma_-^A + \frac{J}{2} (\sigma_x^P \sigma_x^A + \sigma_y^P \sigma_y^A). \quad (7)$$

The coupling strength between the probe qubit and ancilla is  $J$ , whereas the probe and ancilla frequencies are  $\omega^P$  and  $\omega^A$ , respectively. The Pauli matrices are represented by  $\sigma_i$  (with  $i = x, y, \text{ or } z$ ), while  $\sigma_+$  and  $\sigma_-$  are the raising and lowering operators, respectively. The first two terms on the equation's right-hand side, represented by Eq. (7), reflect the self-Hamiltonians for the probe qubit and ancilla, while the following term explains the probe-ancilla interaction. In our design, the ancilla is connected to a fermionic thermal reservoir and is regulated by the Hamiltonian

$$H_R = \omega^R \sigma_+^R \sigma_-^R, \quad (8)$$

where  $\omega^R$  is the frequency corresponding to the reservoir, and the interaction between the ancilla and the reservoir has the following form:

$$H_I = \frac{\eta}{2} (\sigma_x^A \sigma_x^R + \sigma_y^A \sigma_y^R). \quad (9)$$

The symbol  $\eta$  represents the coupling strength between the ancilla and reservoir. The rest of the paper assumes  $\omega^P = \omega^A = \omega^R = \omega$ . The general master equation [34] for the coupled probe-ancilla system, using Born-Markov and secular approximations [30,35], is written as follows:

$$\frac{d}{dt} \rho(t) = -i[H, \rho(t)] + \mathcal{G}^+ \mathcal{D}[\sigma_+^A] + \mathcal{G}^- \mathcal{D}[\sigma_-^A]. \quad (10)$$

Here,  $\mathcal{G}^+ = \Gamma f(\omega)$  and  $\mathcal{G}^- = \Gamma[1 - f(\omega)]$  are the decay rates, where  $\Gamma = 2\pi\eta^2$ , the Fermi-Dirac distribution  $f(\omega) = (e^{\beta\omega} + 1)^{-1}$ , and  $\mathcal{D}[h](\rho) = \sigma_+^A \rho \sigma_-^A$  is the Lindblad dissipator, which is described as

$$\mathcal{D}[h] = h\rho(t)h^\dagger - \frac{1}{2}[h^\dagger h, \rho(t)]_+. \quad (11)$$

In concept,  $[X_1, X_2]_+$  specifies the anticommutator of  $X_1$  and  $X_2$ , and  $\beta$  represents the inverse temperatures (see the Appendix for more details).

In the next section, we will distinguish between the Markovian and non-Markovian regimes in our suggested method. To accomplish this purpose, we shall determine which parameters are important. In fact, manipulating them allows us to induce the non-Markovian regime in our strategy.

### B. Non-Markovianity for a probe in the composite environment

To further recognize the non-Markovian nature of our probe, we will employ an approach based on information flow between the probe system and the composite environment. We use the approach introduced by Breuer *et al.* to assess the degree of non-Markovianity [36],

$$\mathcal{N} = \max_{\rho_{1,2}^{(P)}(0)} \int_{\sigma > 0} dt \sigma(t). \quad (12)$$

The above formula evaluates the presence of feedback or recoherence by examining the change in the rate of the trace

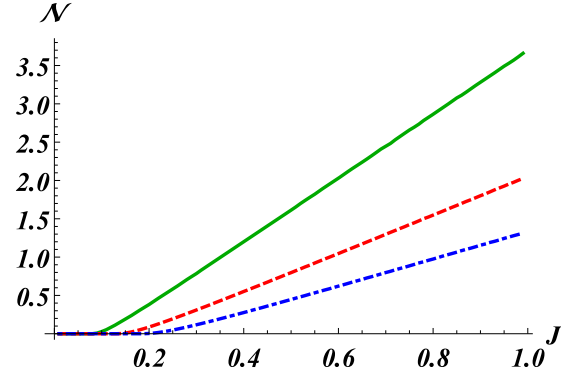


FIG. 2. Non-Markovianity  $\mathcal{N}$  as a function of the coupling strength  $J$  for different values of coupling  $\eta$ . Indeed,  $\eta = 0.22, 0.28, \text{ and } 0.34$  are represented by the green solid, red dashed and blue dot-dashed lines, respectively.

distance between the initial states, where  $\sigma(t) = \frac{d}{dt} \mathcal{D}(t)$  represents the time derivative of the trace distance, such that

$$\mathcal{D}(t) = \frac{1}{2} \text{Tr}\{|\rho_1^{(P)}(t) - \rho_2^{(P)}(t)\}. \quad (13)$$

The trace distance, which reflects the distinguishability of states, shows a continuous decrease over time; i.e., the two states,  $\rho_1^{(P)}(t)$  and  $\rho_2^{(P)}(t)$ , become less distinguishable. In other words, this can be interpreted as a continuous loss of information from the system to the environment, defining Markovian dynamics. Conversely, any temporal increase in the trace distance over time indicates a flow of information from the environment back into the quantum system. This serves as a characteristic signature of memory effects, indicating the non-Markovian nature of the dynamics. Extensive research has demonstrated that for a two-level system, the most appropriate initial states can be selected as a set of orthogonal pure states, such that  $|\pm\rangle = (|0\rangle \pm |1\rangle)/\sqrt{2}$  [37–39].

Figure 2 shows the non-Markovianity measure  $\mathcal{N}$  as a function of  $J$  for various coupling strengths  $\eta$ . The measure  $\mathcal{N}$  is zero for small coupling values  $J$ , implying that the composite environment is Markovian in this regime. Notably, the  $\mathcal{N}$  measure deviates from zero as  $J$  becomes larger. One intriguing discovery is that the degree of non-Markovianity reduces with increasing coupling strength  $\eta$ . This observation strongly suggests that the composite environment becomes completely non-Markovian at higher  $J$  and lower  $\eta$  values. As a result, we will limit further discussion to scenarios in which  $J = 0.99$  in our temperature sensing technique.

## IV. NON-MARKOVIAN QUANTUM THERMOMETRY FOR THE COMPOSITE ENVIRONMENT

Calculations using the density matrix in Eq. (A3) indicate that the analytical expression of  $\mathcal{H}(T)$  is not concise. Furthermore, due to the lack of compact analytical results for the QSNR, the probe's best state is calculated via a numerical technique. Specifically, Fig. 3 illustrates the ratio of the QSNR for different values of temperature  $T$  and for different strategies of initial preparation of the probe state, where  $\mathcal{R}^s$ ,

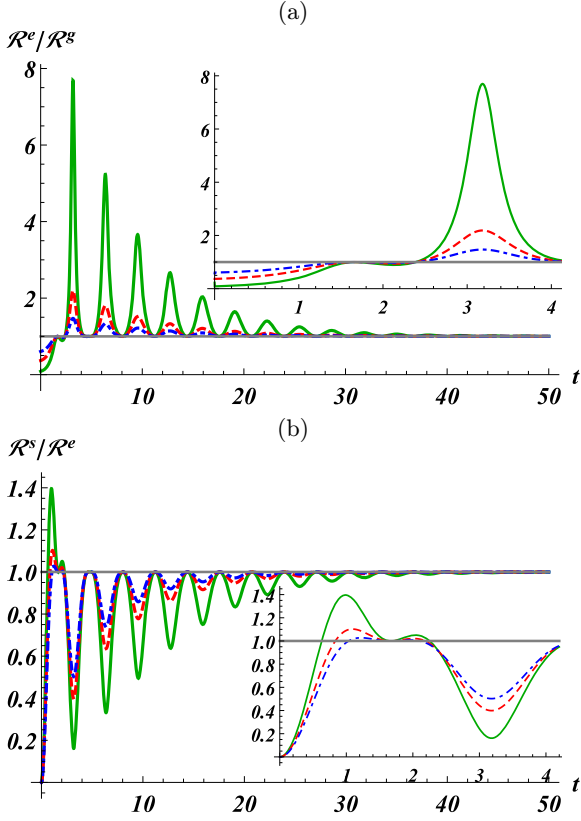


FIG. 3. The ratios of (a)  $\mathcal{R}^e(\theta = \pi)/\mathcal{R}^s(\theta = 0)$  and (b)  $\mathcal{R}^s(\theta = \pi/2)/\mathcal{R}^e(\theta = \pi)$  for different values of temperature, where  $T = 0.5, 1,$  and  $2$  are represented by the green solid, red dashed, and blue dot-dashed lines, respectively. In the insets, we plot the same quantities for small time interaction. Moreover, we set  $J = 0.99$ ,  $\omega = 1$ , and  $\eta = 0.22$ .

$\mathcal{R}^s$ , and  $\mathcal{R}^e$  stand for QSNRs where the probe qubits are prepared initially in the ground, superposed, and excited states, respectively. In all plots, we set  $\omega = 1$  and  $\eta = 0.22$  unless otherwise stated.

The graphs in Fig. 3 highlight that the ideal technique requires preparing the probe in its excited state, i.e.,  $|1\rangle_P$  (shown by the lines with blue dots in the Bloch sphere shown in Fig. 1), although there are certain brief time intervals when this is not the case. As temperature values fall, the ratio  $\mathcal{R}^e/\mathcal{R}^s$  increases, whereas  $\mathcal{R}^s/\mathcal{R}^e$  decreases. For lower temperatures, the ideal preparation state is the excited state ( $|1\rangle_P$ ).

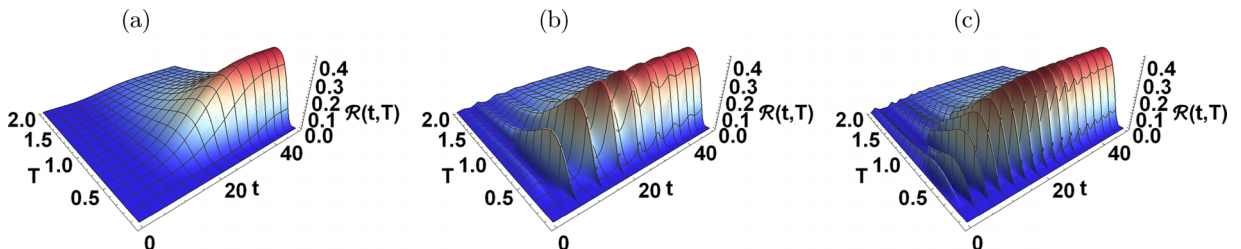


FIG. 4. The QSNR for three distinct coupling values  $J$  as a function of interaction time  $t$  and temperature  $T$ , where  $J = 0.1, 0.5,$  and  $0.99$  for (a)–(c), respectively. Additionally, we set  $\theta = \pi$ ,  $\omega = 1$ , and  $\eta = 0.22$ .

Furthermore, at high values of time interaction, the QSNR becomes  $\theta$  independent. State  $|1\rangle_P$  is deemed the most optimal one based on the approach employed. However, there are some brief time intervals where it is advantageous to prepare the probe in either state  $|0\rangle_P$  or  $(|0\rangle_P + |1\rangle_P)/\sqrt{2}$ . By preparing the probe in its optimal state, namely,  $|1\rangle_P$ , the density matrix of the probe qubit in the Bloch representation reads  $\rho^{(P)}(t) = \frac{1}{2}(\hat{I} + \mathbf{b} \cdot \hat{\sigma})$ . The elements of the Bloch vector are obtained as follows:

$$b_x = 0, \quad b_y = 0, \quad b_z = 2\rho_{11}(t) - 1. \quad (14)$$

In light of the above equation, the explicit expression for the QFI is easily obtained as

$$\mathcal{H}(T) = \frac{(\partial_T b_z)^2}{1 - (b_z)^2}. \quad (15)$$

Expressed in terms of Eq. (5), Fig. 4 illustrates the dynamical behavior of the QSNR as a function of time interaction  $t$  and temperature of the composite environment  $T$  for various values of the strength coupling  $J$ . The results give persuasive evidence that greater coupling  $J$  values result in a more effective improvement of QSNR than lower values of  $J$ , implying that the QSNR behaves significantly  $J$  dependently in nonequilibrium settings. Furthermore, the oscillating patterns of  $\mathcal{R}(t, T)$ , similar to Fig. 2, become more prominent as  $J$  grows. This pattern is especially important for  $J \approx 0.99$ , emphasizing the substantial non-Markovian effects found in Fig. 2. These findings indicate that non-Markovian effects have the potential to increase temperature sensing accuracy in nonequilibrium settings. However, regardless of the magnitude of  $J$ , the QSNR values converge to a single constant value that is exclusively reliant on the temperature of the composite environment in the long-term regime. The highest temperature precision achieved in this context relates to a very low temperature regime, as seen in Fig. 4.

In our approach, nonequilibrium conditions have no effect on the maximum accuracy of the temperature estimation. When the thermometer approaches steady state, the quantum signal-to-noise ratio peaks. The correlation between the probe qubit's steady-state convergence and QSNR maximization has significant implications for quantum thermometry and temperature sensing [40]. This relationship emphasizes the importance of the probe qubit stability in determining the precision and accuracy of temperature measurements utilizing quantum systems. As the probe qubit approaches steady state, the QSNR improves, indicating more sensitivity to tempera-

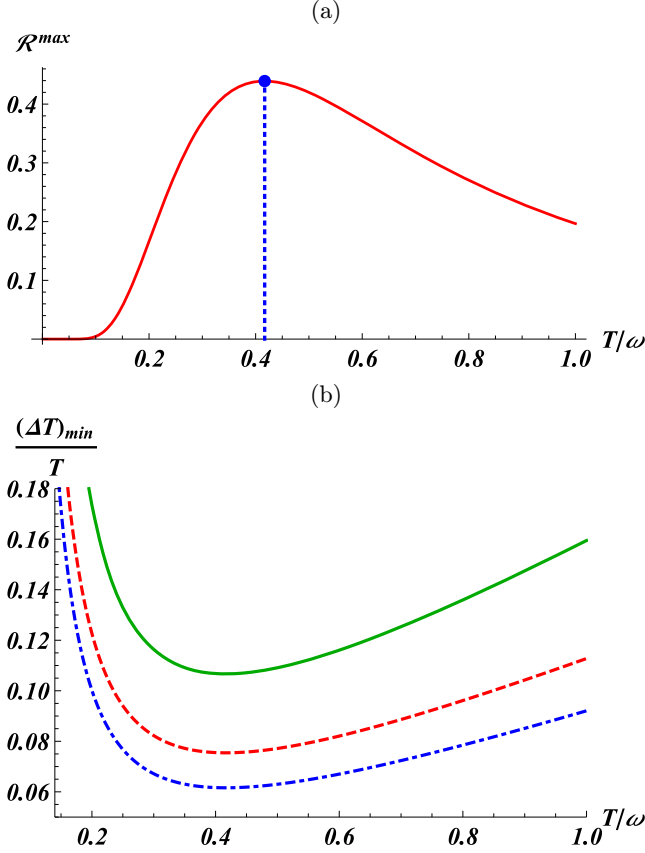


FIG. 5. (a) The maximum QSNR  $\mathcal{R}^{\max}$  as a function of temperature  $T$ . (b) The optimal relative error  $(\Delta T)_{\min}/T$  as a function of temperature  $T$  after 200 (green solid line), 400 (red dashed line), and 600 (blue dot-dashed line) measurements.

ture fluctuations and measurement precision. These results not only provide useful insights for enhancing quantum thermometry techniques but also show a direct relationship between probe qubit stability and temperature measurement accuracy. Particularly, in the equilibrium performance of the thermometer, i.e., the long-time interaction, the QSNR reads

$$\mathcal{R}(T, t \rightarrow +\infty) = \mathcal{R}^{\max} = \frac{\omega^2}{2T^2 \left[ \cosh\left(\frac{\omega}{T}\right) + 1 \right]}. \quad (16)$$

Equation (16) indicates that in the long-time interaction, the QSNR is dependent only on the frequency  $\omega$  and the temperature of the sample itself.

Figure 5(a) exhibits the maximum attainable QSNR as a function of the ratio  $T/\omega$ . It reveals that the QSNR reaches its peak when the ratio  $T/\omega$  is around 0.41. Moreover, the temperature associated with the peak is  $T = 0.41 \omega$ , showing that our sensing procedure performs better at low temperatures. To validate this discovery, Fig. 5(b) depicts the optimal relative error  $(\Delta T)_{\min}/T$  as a function of temperature  $T$  after 200 (green solid line), 400 (red dashed line), and 600 (blue dot-dashed line) measurements. The optimal relative error is temperature dependent in the low-temperature region, implying that our approach may be better suited to the construction of low-temperature quantum sensors. Figure 5(b) shows that

with only 200 measurements, the optimal relative error may be maintained at 17% for the full temperature range (green solid line). After 400 measurements, the ideal relative error stays below 10% for a specified temperature range (red dashed line). As the number of measurements reaches 600, the optimum relative error regularly falls below 10% (blue dot-dashed line).

Our study introduces a single-qubit-based quantum thermometer operating in a non-Markovian composite environment, achieving high precision as measured by QSNR. Remarkably, compared to the dephasing-based method [5] and the Bose-Einstein condensate sensor [41], our approach demonstrates enhanced sensitivity, particularly at low temperatures. However, these methods have an advantage over our method in terms of shorter encoding times.

In the final stage of the temperature sensing protocol, we present a measurement approach that will saturate the quantum Cramér-Rao constraint. It is critical to identify the best measurement for experimental implementation. In this work, we choose a measurement of  $\langle \hat{\sigma}_z \rangle$ . Therefore, for a two-level system, the Fisher information associated with the measurement can be written as [42]

$$\mathcal{F}(T) = \frac{(\partial_T \langle \hat{\sigma}_z \rangle)^2}{\langle \Delta \hat{\sigma}_z^2 \rangle}, \quad (17)$$

where  $\langle \hat{\sigma}_z \rangle$  and  $\langle \Delta \hat{\sigma}_z^2 \rangle$  represent the mean and variance of the measured third Pauli matrix, respectively. The quantum state of the single-qubit temperature sensor, as given by Eq. (A3), is straightforward to derive:

$$\langle \hat{\sigma}_z \rangle = 2\rho_{11}(t) - 1, \quad \langle \Delta \hat{\sigma}_z^2 \rangle = 1 - [2\rho_{11}(t) - 1]^2. \quad (18)$$

According to Eq. (14), we have  $b_z = 2\rho_{11}(t) - 1$ . Thus, the Fisher information for the measurement of  $\hat{\sigma}_z$  is produced by entering the aforementioned equation into Eq. (17):

$$\mathcal{F}(T) = \frac{(\partial_T b_z)^2}{1 - (b_z)^2}. \quad (19)$$

This is identical to the quantum Fisher information given by Eq. (15). Therefore, we can deduce that the sensitivity of the temperature sensor in the current system can saturate the quantum Cramér-Rao bound by conducting the measurement of  $\hat{\sigma}_z$  on the probe qubit.

An attractive feature of our method is that after a period of time, a local measurement on the probe qubit can extract nearly all the information about the temperature. This enhances the feasibility of implementing the thermometer (e.g., a biological sample [43,44]).

## V. SENSING TEMPERATURE OF THE ANCILLA

In this part, we examine a configuration in which the composite environment has varying temperatures. We represent the temperature of the ancilla as  $T_A$  and the temperature of the Markovian reservoir as  $T_R$ . Our goal is to determine the temperature of the ancilla and explore how the reservoir affects it.

Figure 6 displays the QSNR's dynamic behavior for ancilla temperatures ranging from 0.1 to 3, i.e., from the low- to high-temperature regime. It is clear that the QSNR initially

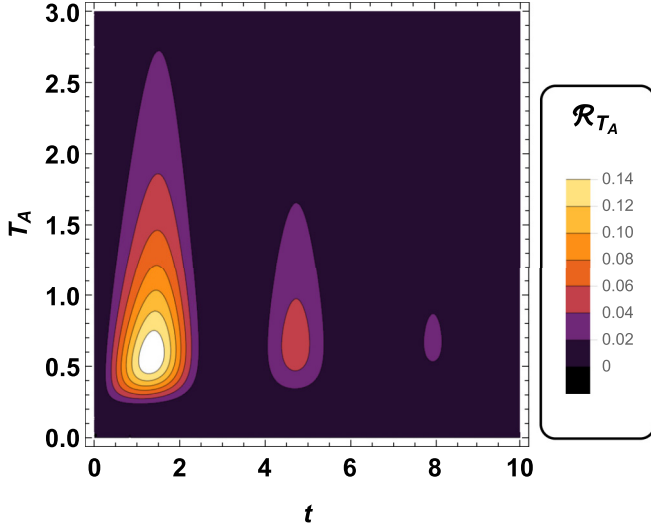


FIG. 6. The QSNR as a function of time interaction  $t$  and temperature  $T_A$  for fixed  $J = 0.99$ ,  $\theta = 0$ ,  $T_R = 1$ ,  $\omega = 1$ , and  $\eta = 0.22$ .

increases and then drops with increased interaction time. Notably, there is a sudden death followed by a QSNR rebirth in the low-temperature regime. This shows that the optimal estimation of the temperature of the ancilla can be accomplished within a finite interaction time  $t_{\text{opt}}$ , i.e., before the probe qubit reaches its stationary state.

Figure 7 provides three plots showing the maximum value of the QSNR, denoted  $\mathcal{R}_{\text{opt}}$ , as a function of the temperature of the ancilla for varying values of  $\theta$ , coupling  $J$ , and reservoir temperature  $T_R$ . However, for specified parameters, namely,  $J = 0.99$  and  $T_R = 1$ , Fig. 7(a) depicts the best technique for preparing the initial state of the probe qubit. The results clearly show that the maximum of the QSNR is attained for low temperatures in the scenario where  $\theta = 0$  [see also the inset in Fig. 7(a)], indicating that the maxima of the QSNR can be boosted by preparing the probe qubit in its ground state. Moreover, Fig. 7(b) exhibits the effect of coupling  $J$  on QSNR (with  $\theta = 0$  and  $T_R = 1$ ). It can be seen that the QSNR in both regimes, low and high temperatures of the ancilla, is substantially dependent on the coupling  $J$  and that as the value of  $J$  grows, so does the maximum precision

in QSNR. Furthermore, precision decreases as the coupling regime transitions from strong to weak. It should be noted that the highest ancilla temperature precision achieved here is for a very low ancilla temperature regime. The temperature of the reservoir is critical to the accuracy of the ancillary temperature estimation. Furthermore, Fig. 7(c), where we set  $\theta = 0$  and  $J = 0.99$ , demonstrates how a high temperature  $T_R$  of the reservoir might boost the maximum of the QSNR.

In Fig. 8, we display the ideal interaction time  $t_{\text{opt}}$ , which is the time when the QSNR reaches its greatest value. However, Fig. 8(a) demonstrates the optimal time interaction as a function of the ancilla temperature  $T_A$  for different probe qubit initializations. The ideal period for low temperatures is clearly dependent on  $\theta$ . When  $\theta = 0$ , the optimal time is smaller at low temperatures and gradually increases with rising ancilla temperature. For high ancilla temperatures, the behavior of  $t_{\text{opt}}$  becomes  $\theta$  independent. In contrast, the coupling  $J$  has a significant influence on the optimal time interaction in both the low- and high-temperature regimes. As the coupling strength  $J$  grows, the optimal time interaction decreases. Furthermore, at low temperatures, a short-time contact between the probe and the composite environment is required for an optimal ancilla temperature estimate. At higher temperatures, however, a long-term interaction between the probe and the composite environment is required to accurately determine the temperature of the ancilla. This suggests that longer contact times is required at high temperatures than at lower temperatures in order to imprint information about the probe's ancilla temperature.

In addition, as expected, the optimal time is smaller for low temperatures compared to high temperatures for all three values of  $J$ , namely, 0.1, 0.5 and 0.99. However, from Figs. 7(b) and 8(b), it is clear that increasing the values of  $J$  leads to an increase in the optimal QSNR [see the inset in Fig. 7(a)], and the optimal time interaction to reach the maximum QSNR decreases as  $J$  increases. Compared to Fig. 2, it is clear that this gain in measurement accuracy follows the same pattern as non-Markovianity. This clearly shows that increased non-Markovianity correlates with greater temperature measurement accuracy. Furthermore, the reservoir temperature  $T_R$  has no effect on  $t_{\text{opt}}$ , indicating that the optimal time interaction is independent of  $T_R$ .

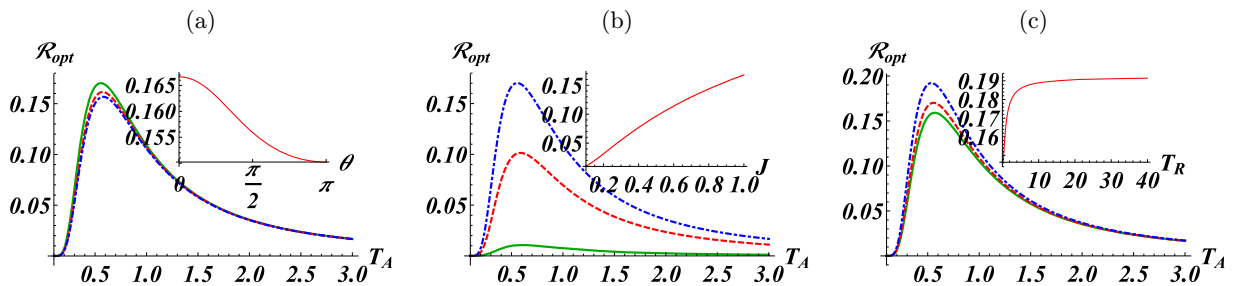


FIG. 7. Plots showing the maximum value of the QSNR  $\mathcal{R}_{\text{opt}}$  in time as a function of the temperature  $T_A$  for (a)  $\theta = 0$  (green solid line),  $\theta = \pi/2$  (red dashed line), and  $\theta = \pi$  (blue dot-dashed line), (b)  $J = 0.1$  (solid green line),  $J = 0.5$  (dashed red line), and  $J = 0.99$  (dot-dashed blue line), and (c)  $T_R = 0.5$  (green solid line), 1 (red dashed line), and 20 (blue dot-dashed line). The insets show the optimal QSNR as a function of  $\theta$  in (a),  $J$  in (b), and  $T_R$  in (c).

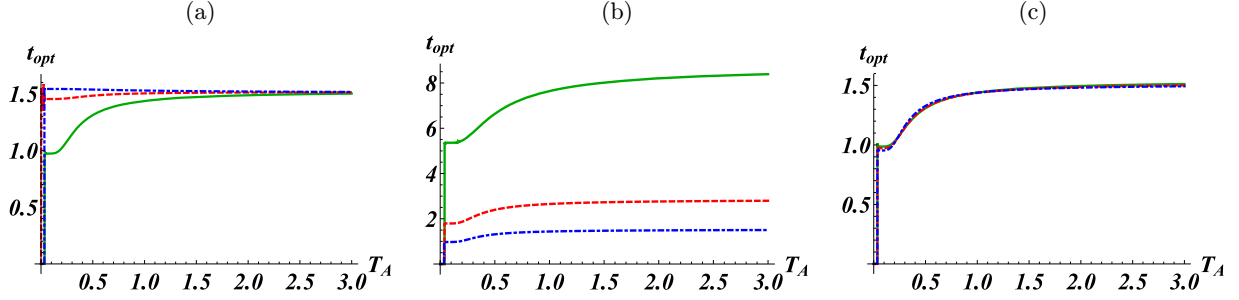


FIG. 8. Plots of the optimal interaction time  $t_{opt}$  versus (a)  $\theta$ , (b)  $J$ , and (c)  $T_R$ .

## VI. CONCLUSION

In this study, we examined single-qubit quantum thermometry with a focus on quantum memory effects and demonstrated its usefulness in estimating the temperature of a composite environment made up of a Markovian reservoir and an ancillary system. We discovered that the highest quantum signal-to-noise ratio occurs when the system approaches steady state, with no observable absolute performance benefit in the nonequilibrium phase. Initially, the probe qubit was better prepared in the excited state than in the ground or superposed states. The non-Markovianity was highly influenced by the probe's nonequilibrium state, increasing with the coupling strength  $J$  and leading to rapid increases with many oscillations in the QSNR, in contrast to the sluggish growth found in the Markovian regime. Furthermore, the QSNR achieves its peak at lengthy interaction periods, relying solely on the temperature of the composite environment. We discovered that the maximum QSNR over the temperature of the composite environment has only one peak, which occurs in the low-temperature regime. This shows that our technique could be better suited to the design of low-temperature quantum sensors. Our suggested method achieves an ideal relative error of less than 17% with only 200 measurements for low temperatures and remains below 10% with 600 measurements.

In addition, we investigated the scenario in which the composite environment has varied temperatures, specifically how the Markovian reservoir influences the temperature estimation of the ancilla. Our findings demonstrated that the QSNR over ancilla temperature reaches its maximum over time for each fixed ancilla temperature value. Furthermore, we emphasized the importance of non-Markovian effects, which might improve the efficiency of ancilla temperature estimates while decreasing the optimal interaction time. A stable temperature in the Markovian reservoir enhanced the maxima of the ancilla temperature estimate when compared to low temperatures. Finally, we demonstrated that an excellent temperature estimate at the quantum limit may be achieved using the feasible strategy of preparing the qubit in an eigenstate of  $\hat{\sigma}_z$  and measuring it after it interacts with the thermal sample.

Our results open up possibilities for future developments, such as the use of entangled probes and the possible adjustment of the interaction Hamiltonian. In addition, our

framework can be expanded by using collisional models. Indeed, the benefits of the latter models come from repeated interactions between a continuous stream of ancillas prepared independently and a system that mediates thermal contact with the environment. However, in terms of potential realizations of our probing scheme, there are several physical platforms that implement a two-level system in structured environments. In fact, examples that include atomic impurities in Bose-Einstein condensates are given in Refs. [45–47], and examples including superconducting qubits are given in Refs. [48,49].

## ACKNOWLEDGMENTS

A.E.A. would like to thank the Max Planck Institute for the Physics of Complex Systems for the financial support and the friendly environment. The authors thank M. G. A. Paris and A. Smirne for useful discussions.

The authors declare that they have no conflict of interest.

## APPENDIX: DERIVATION OF THE MASTER EQUATION

In this Appendix, we provide an exact solution to the master equation used in this paper. To solve the master equation (10), the initial state is

$$\rho(0) = \rho_{\theta}^{(P)} \otimes \rho_{th}^{(A)}, \quad (\text{A1})$$

where  $\rho_{\theta}^{(P)}$  and  $\rho_{th}^{(A)}$  are the probe and ancilla density matrices, respectively, of the following form:

$$\rho^{(P)} = |\psi(\theta)\rangle \langle \psi(\theta)|, \quad \rho_{th}^{(A)} = \frac{e^{-\beta_A H^{(A)}}}{\mathcal{Z}}. \quad (\text{A2})$$

Here,  $\mathcal{Z} = \text{Tr}\{e^{-\beta_A H^{(A)}}\}$  is the partition function of the ancilla, and  $|\psi(\theta)\rangle = \cos(\frac{\theta}{2})|0\rangle + \sin(\frac{\theta}{2})|1\rangle$ , where  $\theta \in [0, \pi]$  and  $\beta_A$  is the inverse temperature of the ancilla. The dynamics of the reduced state of the probe is given by

$$\rho^{(P)}(t) = \text{Tr}_A\{\rho(t)\} = \begin{pmatrix} \rho_{11}(t) & \rho_{12}(t) \\ \rho_{21}(t) & \rho_{22}(t) \end{pmatrix}. \quad (\text{A3})$$

We assume that the ancilla and the reservoir are in thermal equilibrium at temperature  $T$ . Thus, the populations (diagonal) and coherence (off-diagonal) are exactly calculated in our

case as

$$\begin{aligned} \rho_{11}(t) = & \frac{e^{-\frac{1}{2}t(A_1+2\pi\eta^2)}}{4A_2^{3/2}(e^{\omega/T} + 1)} \left\{ 8A_1 e^{\omega/T} [(\pi^2\eta^4 - 4J^2)e^{\frac{1}{2}t(A_1+2\pi\eta^2)} - J^2(e^{\frac{A_1t}{2}} - 1)^2] \right. \\ & + 8A_1 [(\pi^2\eta^4 - 4J^2)e^{\frac{1}{2}t(A_1+2\pi\eta^2)} + J^2(e^{\frac{A_1t}{2}} - 1)^2] \\ & + 8 \cos(\theta) \cosh\left(\frac{\omega}{2T}\right) e^{\frac{A_1t+\omega}{2T}} \left[ -\pi A_2 \eta^2 \sinh\left(\frac{A_1t}{2}\right) + 2A_1(2J^2 - \pi^2\eta^4) \cosh\left(\frac{A_1t}{2}\right) + 4A_1 J^2 \right] \\ & - 4(e^{\omega/T} + 1) \tanh\left(\frac{\omega}{2T}\right) [2\pi\eta^2(e^{A_1t} - 1)(\pi^2\eta^4 - 4J^2)] \\ & \left. - 4(A_1)(e^{\omega/T} + 1) \tanh\left(\frac{\omega}{2T}\right) [(8J^2 - 2\pi^2\eta^4)e^{\frac{1}{2}t(A_1+2\pi\eta^2)} - 8J^2 e^{\frac{A_1t}{2}} + \pi^2\eta^4 e^{A_1t} + \pi^2\eta^4] \right\}, \\ \rho_{22}(t) = & 1 - \rho_{11}(t), \\ \rho_{12}(t) = & \frac{\sin(\theta)e^{-\frac{1}{4}t(2\pi\eta^2+4i\omega)} [2\pi\eta^2 \sinh\left(\frac{A_1t}{4}\right) + A_1 \cosh\left(\frac{A_1t}{4}\right)]}{2A_1} = \rho_{21}^*(t), \end{aligned} \quad (\text{A4})$$

where  $A_1$  and  $A_2$  are given by

$$A_1 = \sqrt{(2\pi\eta^2)^2 - 16J^2}, \quad A_2 = (2\pi\eta^2)^2 - 16J^2. \quad (\text{A5})$$

From Eq. (A4), it becomes evident that the populations, which correspond to the diagonal elements of the density matrix, exhibit a clear dependence on temperature. This temperature dependence indicates that these diagonal elements carry crucial information about the thermal state of the sample. In contrast, the off-diagonal elements, or coherences, remain unaffected by the temperature, implying that they do not encode thermal information. Consequently, by examining the populations of the density matrix, we can infer the temperature of the sample, providing valuable insights into its thermal properties.

- 
- [1] K. Jacobs, *Quantum Measurement Theory and Its Applications* (Cambridge University Press, Cambridge, 2014).
- [2] L. Michalski, K. Eckersdorf, J. Kucharski, and J. McGhee, Temperature measurement, *Meas. Sci. Technol.* **13**, 1651 (2002).
- [3] F. Giazotto, T. T. Heikkilä, A. Luukanen, A. M. Savin, and J. Pekola, Opportunities for mesoscopies in thermometry and refrigeration: Physics and applications, *Rev. Mod. Phys.* **78**, 217 (2006).
- [4] C. D. S. Brites, P. P. Lima, N. J. O. Silva, A. Millán, V. S. Amaral, F. Palacio, and L. D. Carlos, Thermometry at the nanoscale, *Nanoscale* **4**, 4799 (2012).
- [5] S. Razavian, C. Benedetti, M. Bina, Y. Akbari-Kourbolagh, and M. G. A. Paris, Quantum thermometry by single-qubit dephasing, *Eur. Phys. J. Plus* **134**, 284 (2019).
- [6] F. Gebbia, C. Benedetti, F. Benatti, R. Floreanini, M. Bina, and M. G. A. Paris, Two-qubit quantum probes for the temperature of an Ohmic environment, *Phys. Rev. A* **101**, 032112 (2020).
- [7] A. De Pasquale, D. Rossini, R. Fazio, and V. Giovannetti, Local quantum thermal susceptibility, *Nat. Commun.* **7**, 12782 (2016).
- [8] M. Mehboudi, A. Lampo, C. Charalambous, L. A. Correa, M. A. García-March, and M. Lewenstein, Using polarons for sub-nK quantum nondemolition thermometry in a Bose-Einstein condensate, *Phys. Rev. Lett.* **122**, 030403 (2019).
- [9] K. V. Hovhannisyanyan and L. A. Correa, Measuring the temperature of cold many-body quantum systems, *Phys. Rev. B* **98**, 045101 (2018).
- [10] M. Scigliuzzo, A. Bengtsson, J.-C. Besse, A. Wallraff, P. Delsing, and S. Gasparinetti, Primary thermometry of propagating microwaves in the quantum regime, *Phys. Rev. X* **10**, 041054 (2020).
- [11] S. S. Mirkhalaf, D. Benedicto Orenes, M. W. Mitchell, and E. Witkowska, Criticality-enhanced quantum sensing in ferromagnetic Bose-Einstein condensates: Role of readout measurement and detection noise, *Phys. Rev. A* **103**, 023317 (2021).
- [12] D.-J. Zhang and D. M. Tong, Approaching Heisenberg-scalable thermometry with built-in robustness against noise, *npj Quantum Inf.* **8**, 81 (2022).
- [13] M. Brunelli, S. Olivares, M. Paternostro, and M. G. A. Paris, Qubit-assisted thermometry of a quantum harmonic oscillator, *Phys. Rev. A* **86**, 012125 (2012).
- [14] M. Brunelli, S. Olivares, and M. G. A. Paris, Qubit thermometry for micromechanical resonators, *Phys. Rev. A* **84**, 032105 (2011).
- [15] L. Mancino, M. Sbroscia, I. Gianani, E. Rocca, and M. Barbieri, Quantum simulation of single-qubit thermometry using linear optics, *Phys. Rev. Lett.* **118**, 130502 (2017).
- [16] M. M. Feyles, L. Mancino, M. Sbroscia, I. Gianani, and M. Barbieri, Dynamical role of quantum signatures in quantum thermometry, *Phys. Rev. A* **99**, 062114 (2019).
- [17] M. R. Jørgensen, P. P. Potts, M. G. A. Paris, and J. B. Brask, Tight bound on finite-resolution quantum thermometry at low temperatures, *Phys. Rev. Res.* **2**, 033394 (2020).

- [18] Q. Bouton, J. Nettersheim, D. Adam, F. Schmidt, D. Mayer, T. Lausch, E. Tiemann, and A. Widera, Single-atom quantum probes for ultracold gases boosted by nonequilibrium spin dynamics, *Phys. Rev. X* **10**, 011018 (2020).
- [19] M. G. A. Paris, Quantum estimation for quantum technology, *Int. J. Quantum Inf.* **7**, 125 (2009).
- [20] K. El Anouz, A. El Allati, and M. El Baz, Teleporting quantum Fisher information for even and odd coherent states, *J. Opt. Soc. Am. B* **37**, 38 (2020).
- [21] K. El Anouz and A. El Allati, Teleporting quantum Fisher information under Davies-Markovian dynamics, *Phys. A (Amsterdam, Neth.)* **596**, 127133 (2022).
- [22] J. Ma and X. Wang, Fisher information and spin squeezing in the Lipkin-Meshkov-Glick model, *Phys. Rev. A* **80**, 012318 (2009).
- [23] W. Wu and J.-B. Xu, Geometric phase, quantum Fisher information, geometric quantum correlation and quantum phase transition in the cavity-Bose-Einstein-condensate system, *Quantum Inf. Process.* **15**, 3695 (2016).
- [24] F. Fröwis, Kind of entanglement that speeds up quantum evolution, *Phys. Rev. A* **85**, 052127 (2012).
- [25] S. Deffner and S. Campbell, Quantum speed limits: From Heisenberg's uncertainty principle to optimal quantum control, *J. Phys. A* **50**, 453001 (2017).
- [26] X.-M. Lu, X. Wang, and C. P. Sun, Quantum Fisher information flow and non-Markovian processes of open systems, *Phys. Rev. A* **82**, 042103 (2010).
- [27] H. Song, S. Luo, and Y. Hong, Quantum non-Markovianity based on the Fisher-information matrix, *Phys. Rev. A* **91**, 042110 (2015).
- [28] C.-F. Li, G.-C. Guo, and J. Piilo, Non-Markovian quantum dynamics: What does it mean? *Europhys. Lett.* **127**, 50001 (2019).
- [29] K. El Anouz, A. El Allati, and N. Metwally, Different indicators for Markovian and non-Markovian dynamics, *Phys. Lett. A* **384**, 126122 (2020).
- [30] H.-P. Breuer and F. Petruccione, *The Theory of Open Quantum Systems* (Oxford University Press, New York, 2002).
- [31] Y. Aiache, K. El Anouz, N. Metwally, and A. El Allati, Dynamics of quantum coherence and nonlocality of a two-spin system in the chemical compass, *Phys. Rev. E* **109**, 034101 (2024).
- [32] W. H. Zurek, Decoherence, einselection, and the quantum origins of the classical, *Rev. Mod. Phys.* **75**, 715 (2003).
- [33] N. Zhang, C. Chen, S. Y. Bai, W. Wu, and J. H. An, Non-Markovian quantum thermometry, *Phys. Rev. Appl.* **17**, 034073 (2022).
- [34] G. Lindblad, On the generator of quantum dynamical semigroups, *Commun. Math. Phys.* **48**, 119 (1976).
- [35] Y. Aiache, C. Seida, K. El Anouz, and A. El Allati, Treatment of non-Markovian effects to investigate non-locality, dense coding and non-local information, *Phys. Lett. A* **496**, 129320 (2024).
- [36] H. P. Breuer, E. M. Laine, and J. Piilo, Measure for the degree of non-Markovian behavior of quantum processes in open systems, *Phys. Rev. Lett.* **103**, 210401 (2009).
- [37] I. de Vega and D. Alonso, Dynamics of non-Markovian open quantum systems, *Rev. Mod. Phys.* **89**, 015001 (2017).
- [38] S. Wißmann, A. Karlsson, E.-M. Laine, J. Piilo, and H.-P. Breuer, Optimal state pairs for non-Markovian quantum dynamics, *Phys. Rev. A* **86**, 062108 (2012).
- [39] Y. Aiache, S. Al-Kuwari, K. El Anouz, and A. El Allati, Optimal superdense coding capacity in the non-Markovian regime, *J. Phys. A* **57**, 195303 (2024).
- [40] A. Ullah, M. T. Naseem, and Ö. E. Müstecaplıoğlu, Low-temperature quantum thermometry boosted by coherence generation, *Phys. Rev. Res.* **5**, 043184 (2023).
- [41] J.-B. Yuan, B. Zhang, Y.-J. Song, S.-Q. Tang, X.-W. Wang, and L.-M. Kuang, Quantum sensing of temperature close to absolute zero in a Bose-Einstein condensate, *Phys. Rev. A* **107**, 063317 (2023).
- [42] M. T. Mitchison, T. Fogarty, G. Guarnieri, S. Campbell, T. Busch, and J. Goold, *In situ* thermometry of a cold Fermi gas via dephasing impurities, *Phys. Rev. Lett.* **125**, 080402 (2020).
- [43] J.-M. Yang, H. Yang, and L. Lin, Quantum dot nano thermometers reveal heterogeneous local thermogenesis in living cells, *ACS Nano* **5**, 5067 (2011).
- [44] G. Kucsko, P. C. Maurer, N. Y. Yao, M. Kubo, H. J. Noh, P. K. Lo, H. Park, and M. D. Lukin, Nanometre-scale thermometry in a living cell, *Nature (London)* **500**, 54 (2013).
- [45] C. Sabín, A. White, L. Hackermuller, and I. Fuentes, Impurities as a quantum thermometer for a Bose-Einstein condensate, *Sci. Rep.* **4**, 6436 (2014).
- [46] W. K. Mok, K. Bharti, L. C. Kwek, and A. Bayat, Optimal probes for global quantum thermometry, *Commun. Phys.* **4**, 62 (2021).
- [47] P. Haikka, S. McEndoo, G. De Chiara, G. M. Palma, and S. Maniscalco, Quantifying, characterizing, and controlling information flow in ultracold atomic gases, *Phys. Rev. A* **84**, 031602(R) (2011).
- [48] F. Yan *et al.*, The flux qubit revisited to enhance coherence and reproducibility, *Nat. Commun.* **7**, 12964 (2016).
- [49] P. I. Villar and F. C. Lombardo, Decoherence of a solid-state qubit by different noise correlation spectra, *Phys. Lett. A* **379**, 246 (2015).